Molecular Cancer Therapeutics

TSR-033, a Novel Therapeutic Antibody Targeting LAG-3, Enhances T-Cell Function and the Activity of PD-1 Blockade *In Vitro* and *In Vivo*

Srimoyee Ghosh[1], Geeta Sharma[1], Jon Travers[1], Sujatha Kumar[1], Justin Choi[2], H. Toni Jun[2], Marilyn Kehry[2], Sridhar Ramaswamy[1], and David Jenkins[1]

Abstract

Progressive upregulation of checkpoints on tumor-infiltrating lymphocytes promotes an immunosuppressive tumor microenvironment, severely compromising tumor immunity. Lymphocyte activation gene-3 (LAG-3) is a coinhibitory receptor associated with impaired T-cell function and is frequently coexpressed with programmed cell death protein-1 (PD-1) in the context of human cancers. Targeting LAG-3 in conjunction with PD-1 thus represents a strategy to amplify and broaden the therapeutic impact of PD-1 blockade alone. We have generated a high affinity and selective humanized monoclonal IgG4 antibody, TSR-033, which binds human LAG-3 and serves as a functional antagonist, enhancing *in vitro* T-cell activation both in mixed lymphocyte reactions and staphylococcal enterotoxin B-driven stimulation assays. In a humanized mouse non–small cell lung carcinoma model, TSR-033 boosted the antitumor efficacy of PD-1 monotherapy, with a concomitant increase in immune activation. Analogous studies in a murine syngeneic tumor model using surrogate antibodies demonstrated significant synergy between LAG-3 and PD-1 blockade—combination treatment led to a marked improvement in therapeutic efficacy, increased T-cell proliferation, IFNγ production, and elicited durable immunologic memory upon tumor rechallenge. Taken together, the pharmacologic activity of TSR-033 demonstrates that it is a potent anti-LAG-3 therapeutic antibody and supports its clinical investigation in cancer patients.

Introduction

Tumor persistence leads to sustained exposure of T cells to neoantigens—this results in repeated cycles of activation which culminate in a state of severe T-cell dysfunction or exhaustion, characterized by distinct epigenetic and transcriptional profiles (1–3). Chronic T-cell exhaustion is marked by the progressive upregulation of coinhibitory receptors, PD-1 being one of the most prominent, but also other coregulated receptors such as LAG-3 (4, 5).

LAG-3 is a transmembrane protein of the Ig superfamily, expressed on a host of immune cell subtypes, including T cells, natural killer (NK) cells, dendritic cells (DC), monocytes, macrophages, and B cells (4, 6, 7). LAG-3 has structural homology with the CD4 coreceptor and binds MHC Class II with higher affinity than CD4, although other ligands such as LSECtin have been also identified (8–10). LAG-3 engagement on the T-cell surface leads to attenuation of T-cell activation, proliferation, and cytokine production, downstream signaling being dependent on a conserved KIEELE motif in the LAG-3 cytoplasmic tail (4).

Consistent with this immunomodulatory role, LAG-3 marks chronically exhausted or dysfunctional T cells in cancer, particularly within the tumor microenvironment relative to peripheral blood (11–13). LAG-3 is frequently coexpressed with PD-1 on tumor-infiltrating lymphocytes (TIL) across several tumor types (11, 14–17). LAG-3 colocalizes with PD-1 at the immunologic synapse following T-cell receptor (TCR) triggering, also being associated with the signaling complex of PD-1 and the inhibitory phosphatases SHP-1/SHP-2 [Src-homology 2 domain (SH2)-containing protein tyrosine phosphatases], which act to attenuate the TCR activation signal (18). Further, genetic ablation of LAG-3 accentuates the autoimmune phenotype of *Pdcd1* (PD-1) knockout mice, also increasing the susceptibility of $Lag3^{-/-}Pdcd1^{-/-}$ double knockout animals to tumor growth in syngeneic models (19). The spatio-temporal, transcriptional, and functional correlation between PD-1 and LAG-3 underscores the rationale for combined blockade of both PD-1 and LAG-3 as an immunotherapeutic approach in the context of human cancers.

Despite the clinical success of checkpoint therapy targeting the PD(L)-1 axis, particularly in malignancies such melanoma, NSCLC, and renal carcinoma (20, 21), a sizeable proportion of patients demonstrate resistance (22, 23). Alternative checkpoint receptors such as LAG-3 have been implicated in resistance to PD(L)-1 inhibition, wherein the full extent of immuno-stimulation resulting from PD(L)-1 blockade is restricted either by the concurrent expression of other checkpoints (primary resistance) or by their secondary upregulation in response to PD(L)-1 blockade (adaptive resistance; ref. 23). Targeting LAG-3 in addition to PD-1, thus represents a strategy for broadening the therapeutic scope of anti-PD-1 monotherapy by intensifying the immune invigoration elicited by PD-1 blockade alone.

[1]TESARO, Inc., Waltham, Massachusetts. [2]AnaptysBio, San Diego, California.

Note: Supplementary data for this article are available at Molecular Cancer Therapeutics Online (http://mct.aacrjournals.org/).

Corresponding Author: Srimoyee Ghosh, TESARO, Inc., Waltham, MA 02451. Phone: 781-257-2286; E-mail: sghosh@tesarobio.com

doi: 10.1158/1535-7163.MCT-18-0836

Materials and Methods

Antibodies

Rat antibodies from hybridomas were engineered as chimeric rat/mouse antibodies using wild-type mouse κ light chain and mouse γ1 heavy chain with the D265A mutation to eliminate murine Fcγ receptor (FcγR) binding (24). The rationale for this is to prevent depletion of PD-1$^+$ or LAG-3$^+$ cells by complement-dependent or antibody-dependent cell cytotoxicity (CDC or ADCC) in the *in vivo* syngeneic tumor model. Specifically, anti-mouse PD-1 [chimeric RMP1-14 (25) engineered as a mouse IgG1, κ with a D265A mutation in the heavy chains] and anti-mouse LAG-3 [chimeric C9B7W (26) engineered as a mouse IgG1, κ with a D265A mutation in the heavy chains] were expressed in stably transfected CHO-S cells (ATCC) grown in FreeStyle CHO Expression Medium (ThermoFisher), and purified using protein A affinity chromatography (rProtein A Sepharose FF, GE).

TSR-033 was derived from a mouse mAb (obtained by immunization of mice with both human and cyno LAG-3) by grafting the heavy chain and light chain complementarity determining regions (CDR) onto the germline frameworks of their nearest human orthologues, followed by maturation via mammalian cell display and somatic hypermutation, using the AnaptysBio SHM-XEL system (27, 28). TSR-033 and TSR-042 (29) are both human IgG4 antibodies, produced in CHO-K1 cells (ATCC) in Dynamis media (ThermoFisher) and purified using Protein A affinity capture (Eshmuno A Resin, Millipore, Sigma). This isotype was selected as a backbone to militate against potential clearance of tumor-reactive T cells expressing PD-1/LAG-3 because IgG4 antibodies do not activate complement and exhibit reduced binding to low-affinity human FcγRs, resulting in them typically not displaying appreciable CDC or ADCC (30, 31). A comparison of the attributes of the mouse and human antibodies is provided in Supplementary Table S1.

A20 lymphoma model

BALB/c mice (Taconic) were acclimated as per the Institutional Animal Care and Use Committee (IACUC) guidelines and implanted with 0.2×10^6 A20 cells (ATCC) subcutaneously in the right flank. A20 cells were freshly thawed and expanded for inoculations—before inoculation, the cell line was tested for mycoplasma using MycoAlert Mycoplasma Detection Kit (Lonza). The mice were randomized into four groups of 10 mice each at tumor volumes of 30 to 50 mm^3 and dosed intraperitoneally with antibody (10 mg/kg) starting on the day of randomization. Groups were dosed with either a mouse IgG1 isotype control antibody, anti-mouse PD-1, anti-mouse LAG-3 (described in preceding section), or a combination of both. Tumor and body weight measurements were collected twice weekly, and tumor volumes were calculated using the equation $(L \times W^2)/2$, where L and W refer to the length and width dimensions, respectively. The treatment continued twice weekly and mice were euthanized as individual tumors reached volumes >2,000 mm^3. The general health of mice was monitored daily and all experiments were conducted in accordance with the Association for Accreditation of Laboratory Animal Care and IACUC guidelines. The mice with complete regression were re-challenged after a gap of 4 weeks with the same number of A20 cells implanted subcutaneously in the opposite flank. Six additional naïve mice were also implanted simultaneously as controls. The mice were monitored until tumors reached volumes >2,000 mm^3.

LAG-3 binding assays

Whole blood from healthy human donors ($n = 3$; identified through screening of a panel of donors for appreciable LAG-3 expression by FACS) was incubated overnight with increasing concentrations of TSR-033, followed by isolation of PBMCs using Ficoll density gradient separation, staining with antibodies to human CD4, CD8 (Biolegend), and LAG-3 (REA351; Miltenyi). Bound TSR-033 on the surface of CD4 and CD8 T cells was detected using anti-human IgG4:PE (Southern Biotech) by flow cytometry.

MHC Class II binding assay

Increasing concentrations of TSR-033 (or isotype control) ranging from 0.04 to 300 nmol/L were first incubated with a fixed concentration (3 nmol/L) of a fluorescently labeled LAG-3 fusion protein [DyLight (Dyl)-650 LAG-3 huIgG1-Fc]. LAG-3 fusion protein/antibody mixtures were then added to Daudi cells for 30 minutes on ice. After washing to remove unbound protein, the samples were analyzed on a BD FACS Array (BD Biosciences) and the data were analyzed using FlowJo software. LAG-3 binding was assessed by monitoring cell-associated Dyl-650 fluorescence.

NFAT reporter assay

Jurkat cells were engineered to express LAG-3 and a luciferase reporter driven by an NFAT response element (NFAT-RE) (CS194820; Promega) and co-cultured with MHC Class II expressing Raji cells in the presence of checkpoint inhibitors or isotype control (as per manufacturer's instructions). NFAT-RE–mediated luminescence was monitored on a Synergy HTX plate reader (BioTek Instruments) to assess the extent of T-cell stimulation.

MLR

Monocyte-derived DCs were differentiated from peripheral blood monocytes isolated from a set of healthy human donors by 7 days of culture with GM-CSF and IL4. CD4 T cells were isolated from peripheral blood of a different set of healthy human donors (Miltenyi). DCs from one donor and CD4 T cells from a second donor were incubated in the presence of TSR-033, TSR-042 (anti-human PD-1 antagonist antibody), or isotype control antibody for 48 hours, and T-cell activation was measured by quantifying secreted IL2. The culture medium was removed after short centrifugation and stored at −80°C until analysis for IL2 levels by ELISA (R&D Systems Duo Set for human IL2).

SEB stimulation

PBMCs from healthy human donors ($n = 5$) were plated at 100,000 cells/well in 96-well flat-bottomed plates and stimulated with 100 ng/mL SEB for 3 days in the presence of checkpoint inhibitors or isotype control, followed by measurement of IL2 in cell culture supernatants using a cytometric bead array (CBA; BD Biosciences). PD-1 and LAG-3 expression on individual donors following SEB stimulation was verified using flow cytometry.

A549 HuNOG-EXL NSCLC tumor model

Twelve-week-old HuNOG-EXL mice (highly immunodeficient NOG mice expressing human GM-CSF and human IL3, engrafted with CD34$^+$ human hematopoietic stem cells) were procured from Taconic Biosciences. Taconic's HuNOG-EXL engraftment criteria for batch release is >25% human CD45$^+$ cells in the peripheral blood; all mice for our study had 55% to 65% human CD45$^+$ cells when received. HuNOG-EXL mice are associated

with improved cellularity and engraftment (lymphoid and myeloid), with IL3/GM-CSF providing additional support for the development myeloid sublineages (30–32). Mice were acclimated as per the IACUC guidelines before implantation with A549 cells. The A549 cell line (derived from human lung adenocarcinoma; ref. 33) was procured from ATCC (ATCC CCL-185; Manasses), freshly thawed, and grown in monolayer culture in RPMI1640/10% FBS in a 37°C incubator with 5% CO_2. The cells were expanded in T-160 flasks, harvested by trypsinization on the day of inoculation, and 5×10^6 A549 cells were implanted subcutaneously in the right flank of each mouse. Prior to inoculation, the cell line was tested for mycoplasma using MycoAlert Mycoplasma Detection Kit (Lonza). Mice were randomized at tumor volumes between 80 and 120 mm^3 into four groups of five mice each. Each group was administered either human IgG4 isotype control, TSR-042, TSR-033, or a combination of TSR-042 and TSR-033 intraperitoneally at a dose of 10 mg/kg twice weekly throughout the study duration. Tumor and body weight measurements were collected twice weekly, and tumor volumes were calculated using the equation $(L \times W^2)/2$, where L and W refer to the length and width dimensions, respectively. The general health of mice was monitored daily, and all experiments were conducted in accordance with the Association for Accreditation of Laboratory Animal Care and the IACUC guidelines. The mice were euthanized a day after the last dose, tumors, and spleens were collected in ice cold RPMI1640 and processed immediately for flow cytometry. Additionally, HuNOG-EXL mice were analyzed in-house at day 10 post-inoculation to ensure sustained engraftment of human CD45 cells and in order to profile T, NK, and myeloid cell populations (Supplementary Fig. S1).

Tumor processing and flow cytometry

Tumors were disaggregated using the GentleMACS Mouse Tumor Dissociation Kit (Miltenyi). Spleens were dissociated through a 70 μm nylon cell strainer and resuspended in red blood cell lysis buffer (Sigma) for 1 minute. All cells were then stained with a viability dye (Thermo Fisher) and Fc block (eBioscience) before staining with fluorophore-conjugated antibodies in flow cytometry staining buffer. The cells were stained for T-cell markers including CD45, CD3, CD4, CD8, FOXP3, CCR7, Ki67, and CD45RA (eBioscience). Intracellular staining was performed using the FOXP3/transcription factor staining buffer set (eBioscience) and cells were fixed. Myeloid markers included CD68, HLA-DR, CD33, CD209, and CD56. Counting beads (123Count eBeads; eBioscience) were added to the samples before acquisition on an LSRII (BD Biosciences) and analysis was done using FlowJo (TreeStar).

Statistical analysis and calculations

Unpaired one-tailed Student T test was used to assess differences between immune cell frequencies in mice that received anti-PD-1+anti-LAG-3 combination therapy, relative to anti-PD-1 monotherapy and $P \leq 0.05$ was considered significant. Tumor growth inhibition (TGI) at termination was calculated using the following formula: $100 \times (1 - T_t/T_0)$, where T_t and T_0 are the average tumor volumes for a given treatment arm and for isotype control, respectively. Coefficient of drug interaction (CDI) at termination was calculated using the following formula: $z/(x^*y)$, where z equals ratio of average tumor volume of combination group to control; x and y equal ratios of average tumor volumes for either monotherapy arm to control. CDI = 1 indicates additivity whereas CDI < 1 indicates synergism and CDI < 0.7 indicates significant synergy (34, 35).

Results

Striking efficacy of combined LAG-3+PD-1 blockade in a syngeneic mouse tumor model

Cooperativity or an additive effect of LAG-3+PD-1 blockade in impeding tumor growth has been demonstrated in several syngeneic tumor models, notably in models of ovarian cancer, melanoma, sarcoma, and colon carcinoma (18, 19, 36). We first evaluated antitumor responses elicited by LAG-3+PD-1 checkpoint blockade in the mouse A20 lymphoma tumor model—A20 cells are known to express high levels of murine MHC Class II, given their B-cell origin, and also PD-L1 (37). A20 cells were subcutaneously implanted into BALB/c mice, and dosing commenced twice weekly once the tumors became palpable with mouse anti-PD-1, anti-LAG-3, the combination, or an IgG1 isotype control. Tumor growth was monitored for 35 days until all animals in the isotype control group (10/10) were euthanized due to increased tumor burden (Materials and Methods). Although we observed relatively high efficacy in the monotherapy arms (TGI of 64% and 68% respectively for anti-PD-1 and anti-LAG-3 on day 35), the combination of anti-PD-1+anti-LAG-3 demonstrated significant synergy, abrogating tumor growth in a majority of the implanted mice (TGI of 97% on day 35; coefficient of drug interaction, CDI < 0.7; Fig. 1A). In the anti-PD-1 and anti-LAG-3 treatment groups, 2/10 and 1/10 animals respectively, reached the end-point tumor volume, whereas there were no animal losses in the combination treatment arm. There were statistically significant reductions in average tumor volumes for mice on all three treatment arms, relative to isotype control ($P \leq 0.05$, Student T test). Mouse spleens were isolated on day 35 ($n = 4$ per group) and assessed for immune cell populations by flow cytometry. Compared with the anti-PD-1 treatment group, the animals on combination therapy, had significant increases in proliferating T cells and total CD8 T cells in their spleens, correlating with the improved tumor outcomes observed in this group (Fig. 1B).

Immunologic memory generated by checkpoint blockade

To evaluate the impact of administering anti-LAG-3 alongside anti-PD-1 monotherapy on antitumor immune memory, we monitored surviving mice in the anti-PD-1 (4/10) and combination therapy (6/10) groups for tumor-free survival for an additional 4 weeks and re-challenged these mice with the original number of A20 cells (no surviving animals in either the isotype control or anti-LAG-3 monotherapy groups; Materials and Methods). Naïve BALB/c mice were simultaneously implanted as positive controls for A20 tumor growth (Fig. 1C). The *de novo* inoculated mice all developed tumors, which rapidly reached the endpoint volume, whereas the re-challenged animals remained tumor-free at the end of 6 weeks, suggesting that tumor-free survival was accompanied by the establishment of immunologic memory, elicited by both the initial anti-PD-1 or anti-PD-1+anti-LAG-3 antibody treatment (Fig. 1C). Although both groups uniformly rejected tumors upon re-challenge, the animals in the combination group had significantly higher frequencies of CD4 and CD8 effector-memory T cells as well as IFNγ-producing T cells in their spleens, suggestive of more potent immuno-stimulation elicited by combining LAG-3 blockade with PD-1 inhibition (Fig. 1D). The synergistic improvement in antitumor efficacy and

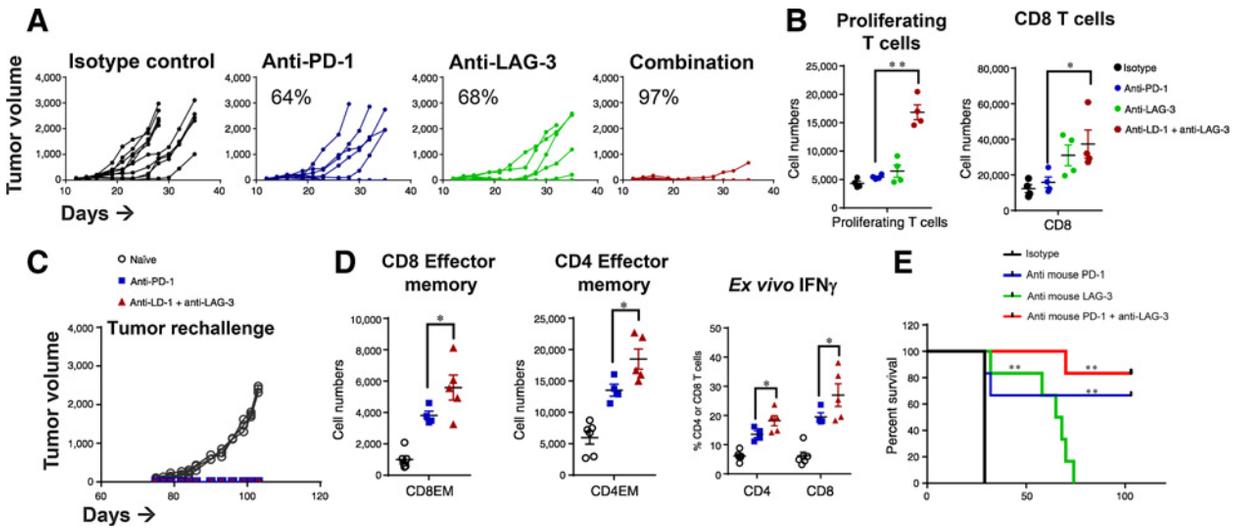

Figure 1.

Simultaneous blockade of LAG-3 and PD-1 synergizes to elicit increased efficacy, immune stimulation, and immunologic memory in mouse A20 lymphoma model. **A,** A20 cells were implanted subcutaneously into Balb/c mice, and tumors were grown to 30 to 50 mm^3 before randomization ($n = 10$ per group) for treatment with either isotype control, anti-LAG3, anti-PD-1, or the combination (10 mg/kg, twice weekly; Materials and Methods); coefficient of drug interaction, CDI <0.7 (significant synergy). **B,** Mice ($n = 4$ per group) were sacrificed on day 36, and pharmacodynamic changes in immune cells in the spleen were assessed. The combination group displayed a significant increase in proliferating T cells and total CD8 T cells, relative to anti-PD-1 treatment alone. **C,** Surviving animals in each group were monitored for tumor-free survival for 40 days, followed by rechallenge with A20 cells ($n = 4$ and $n = 6$, for anti-PD-1 and combination treatment groups, respectively). Naïve mice ($n = 6$) were inoculated in parallel and monitored for tumor growth. **D,** Significant increase in effector-memory ($CD44^+CD62L^-$) T cells in the combination group and higher proportion of splenic $IFN\gamma^+$ CD8 T cells, compared with PD-1 blockade alone. Mice were sacrificed on day 41 post-rechallenge and spleens assessed for immune cell populations by flow cytometry; *, $P \leq 0.05$; **, $P \leq 0.01$, unpaired Student *T* test. **E,** Kaplan–Meier survival curves for treatment arms; **, $P \leq 0.01$ by the log-rank (Mantel–Cox) test, relative to isotype control.

increased T-cell activation observed with PD-1/LAG-3 dual inhibition in the A20 syngeneic model are in line with reports from multiple mouse tumor models (36). Coupled here with the apparent generation of a memory response, these findings bolster preclinical rationale for combining LAG-3 blockade with PD-1 monotherapy. Interestingly, all lines of therapy had a significant effect on prolonging mouse survival relative to isotype control for the entire duration of the study, with the combination arm achieving maximum benefit (Fig. 1E). There was no significant difference between survival curves of the anti-PD-1 alone versus combination treatment arms (Fig. 1E).

Generation of a high affinity therapeutic antibody targeting human LAG-3

TSR-033 is a high affinity humanized IgG4, κ mAb that specifically binds LAG-3 and blocks the interaction between LAG-3 and its ligand MHC Class II. TSR-033 was derived from a mouse mAb by humanization followed by maturation via mammalian cell display and somatic hypermutation using the AnaptysBio SHM-XEL system (27, 28). In addition, the constant region contains a stabilizing mutation in the hinge region, S228P, which prevents *in vivo* half molecule exchange with other IgG4 antibodies and improves IgG4 *in vivo* half-life and tissue distribution (38).

Binding of TSR-033 to LAG-3

TSR-033 was characterized by surface plasmon residence (SPR) for binding to recombinant human and cynomolgus monkey (cyno) LAG-3 Fc fusion proteins (Table 1; K_D values of 0.95 and 2.0 nmol/L, respectively). Binding kinetics for human and cyno LAG-3 were similar, with less than a two-fold difference in association/dissociation rates and a two-fold difference in K_D values by SPR. In addition, binding of TSR-033 to human or cyno LAG-3 expressed on the cell surface of Chinese hamster ovary (CHO)-S cells was assessed by flow cytometry using an Alexa Fluor 647-conjugated goat anti-human IgG F(ab')2 to detect antibody binding (Fig. 2A; Table 1). TSR-033 bound to cell surface human and cyno LAG-3 with EC_{50} values of 0.8 and 2.6 nmol/L, respectively. TSR-033 did not bind to cell surface-expressed mouse LAG-3 or to recombinant mouse and rat LAG-3 as assessed by SPR

Table 1. TSR-033 binding to LAG-3 by surface plasmon resonance (SPR) and LAG-expressing CHO cells

	Kinetic parameters (SPR)[a]			LAG-3–expressing CHO cells[b]	
Species	K_{assoc} (milliseconds)$^{-1}$	K_{dissoc} (seconds)$^{-1}$	K_D (nmol/L)	EC_{50} (nmol/L)	EC_{90} (nmol/L)
Human LAG-3	1.3×10^5	1.25×10^{-4}	0.95	0.8	11.9
Cynomolgus LAG-3	1.1×10^5	2.3×10^{-4}	2.0	2.6	68.5

[a]K_{assoc}, association rate constant; K_{dissoc}, dissociation rate constant; K_D, dissociation constant.
[b]TSR-033 binding not detected on nontransfected CHO cells.

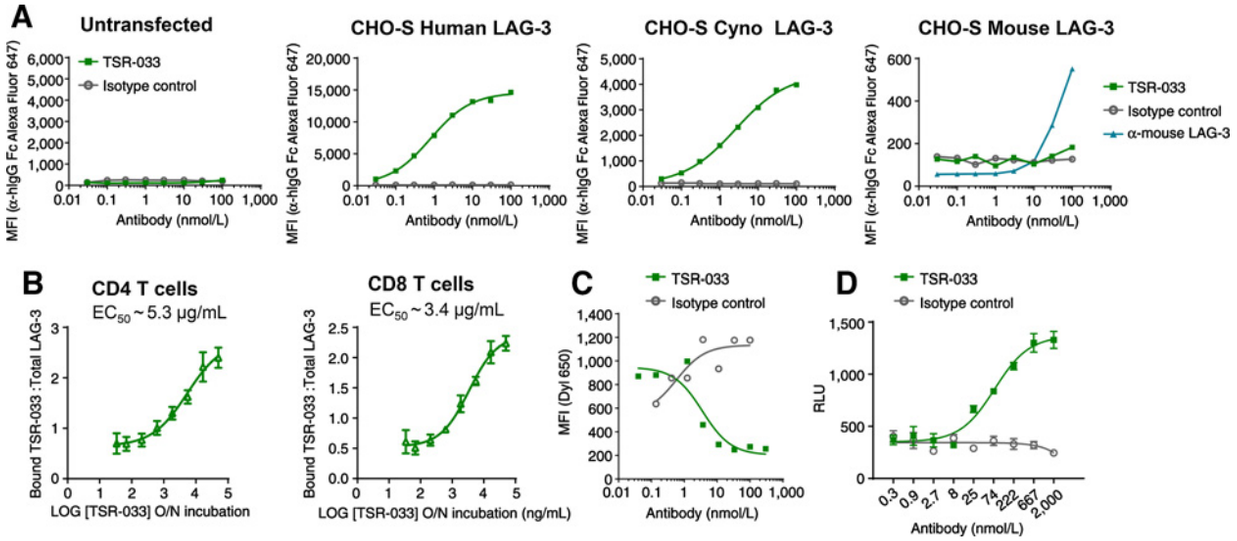

Figure 2.

TSR-033 binds with high affinity to human and cyno LAG-3. **A,** TSR-033 binds human and cyno LAG-3 expressed on the surface of CHO-S cells, but not mouse LAG-3, as assessed by flow cytometry. **B,** TSR-033 binds LAG-3 on resting CD4 and CD8 T cells in health human donors ($n = 3$); total LAG-3 was detected using a noncompeting antihuman LAG-3 antibody (Materials and Methods). **C,** TSR-033 inhibits binding of labeled LAG-3 Fc fusion protein to MHC Class II expressing Daudi cells. **D,** TSR-033 relieves LAG-3–mediated repression of an NFAT-responsive element, downstream of TCR signaling. Data are representative of at least two separate occasions.

(Fig. 2A; Supplementary Fig. S2). These findings are consistent with the degree of amino acid sequence identity observed between the extracellular domain of human LAG-3, relative to cyno (93%) and mouse (70%) LAG-3. TSR-033 binding to endogenous LAG-3 on human T cells was confirmed by overnight incubation of whole blood from healthy human donors with TSR-033, followed by isolation of peripheral blood mononuclear cells (PBMC) and the simultaneous detection of bound TSR-033 using a PE-conjugated anti-human IgG4 and total LAG-3 by flow cytometry (Materials and Methods; raw ratio of mean fluorescence intensity of bound TSR-033 to total LAG-3; Fig. 2B).

TSR-033 blocks LAG-3 binding to MHC Class II on Daudi cells

LAG-3 binds MHC Class II, as demonstrated in quantitative cell adhesion assays with LAG-3 transfectants and MHC Class II expressing B cell lines (10, 39). Cell adhesion was dependent on the LAG-3:MHC Class II interaction, and was disrupted by both anti-LAG-3 and anti-MHC Class II blocking antibodies (39). We used a flow cytometry-based version of this assay, measuring the binding of a fluorescently labeled LAG-3 Fc fusion protein to Daudi cells which express high levels of MHC Class II (40). Preincubation of labeled LAG-3 with increasing concentrations of TSR-033 led to a dose-dependent inhibition of LAG-3 binding to Daudi cells, assessed by monitoring cell-associated fluorescence by flow cytometry (Fig. 2C). We measured the functional effect of disrupting the LAG-3:MHC Class II interaction in a T-cell activation reporter bioassay, using MHC Class II-expressing Raji cells and LAG-3–expressing Jurkat cells, the latter also transfected with a nuclear factor of activated T cells (NFAT) responsive luciferase reporter gene (Materials and Methods). TSR-033 relieved LAG-3–mediated repression of T-cell stimulation, as measured by a dose-dependent increase in luminescence as a consequence of enhanced NFAT triggering, directly downstream of T-cell activation (Fig. 2D).

TSR-033 increases IL2 production in *in vitro* T-cell activation assays

The functional antagonist activity of TSR-033 was evaluated in a human CD4 T-cell MLR assay, either singly or in combination with anti-PD-1 (TSR-042; ref. 29). Primary human CD4 T cells isolated from healthy human donors were co-cultured with monocyte-derived DCs from a different set of donors (41). Allogeneic stimulation of T cells typically leads to the upregulation of checkpoints such as PD-1 and LAG-3 during the course of the MLR assay, dampening the magnitude of T-cell activation (42). DCs and allogeneic CD4 T cells were incubated in the presence of TSR-033 or isotype control for 48 hours and T-cell activation was quantified by the level of IL2 secreted. Antagonism of LAG-3 by TSR-033 increased IL2 production ($EC_{50} = 2.3$ nmol/L; Fig. 3A), whereas combination of TSR- 033 with a constant low concentration of TSR-042 (anti-PD-1 antagonist antibody; refs. 29, 43) at 13 and 133 pmol/L (MLR EC_{10} and EC_{50} concentrations for TSR-042, respectively; ref. 29), led to further de-repression of T-cell activation with EC_{50} values of 640 and 170 pmol/L for TSR-033, respectively (Fig. 3B).

We tested the immuno-stimulatory capacity of TSR-033 in an orthogonal assay system in which healthy human donor PBMCs were stimulated for 3 days with SEB, followed by the measurement of IL2 secretion in the culture supernatant (Fig. 3C). Addition of TSR-033 to SEB-stimulated PBMCs led to increased IL2 production, albeit to a lesser extent than the addition of TSR-042 alone, whereas the TSR-033+TSR-042 combination had the strongest effect, highlighting the importance of counteracting both co-inhibitory pathways for robust T-cell activation (Fig. 3C).

Increased efficacy of combination therapy in an NSCLC humanized mouse model

LAG-3 is expressed on TILs in patients with NSCLC and is correlated both with PD-1 expression and poor prognosis (44).

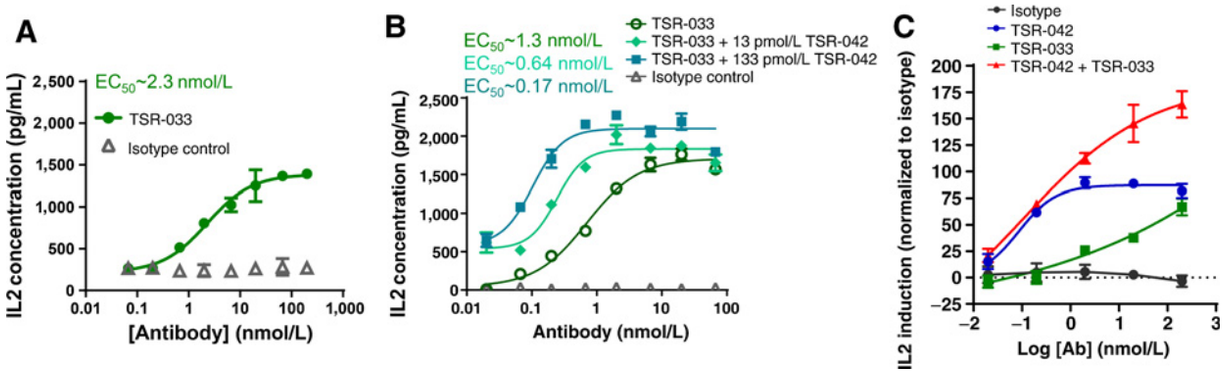

Figure 3.

TSR-033 amplifies T-cell effector function, particularly in combination with anti-PD-1. The functional activity of TSR-033 was evaluated in an MLR assay, in which primary human CD4 T cells were mixed with monocyte-derived dendritic cells from a different donor. In these studies, dendritic cells and allogeneic CD4 T cells were incubated (**A**) in the presence of TSR-033 or isotype control or (**B**) TSR-033, TSR-042, and isotype control at indicated concentrations for 48 hours, and activation of T cells was determined by measuring the level of IL2 secretion. **C,** The ability of TSR-033 and TSR-042 to induce IL2 from human PBMCs ($n = 5$ donors) stimulated with 100 ng/mL SEB for 3 days was assessed. Data are representative of at least two separate occasions.

In vivo antitumor activity of TSR-033, TSR-042, or the combination was tested using humanized NOG-EXL mice, subcutaneously implanted with the human NSCLC A549 cell line (32). Mice were dosed twice weekly with mono- or combination therapy and monitored for tumor growth (Fig. 4A). Compared with an IgG4 isotype control, both TSR-042 and TSR-033 monotherapy had a modest effect on tumor growth (TGI of 26% and 23%, respectively at termination; Fig. 4A). The combination of TSR-033 with TSR-042 produced an additive effect, impeding tumor growth to a greater extent compared with either monotherapy (TGI of 45% at termination). There were no significant differences between survival curves for TSR-042, TSR-033, or the combination, relative to isotype control (Supplementary Fig. S3). The antitumor effect here is different from the striking synergy observed in the A20 syngeneic model (Fig. 1A), and could, at least partially, be attributable to delayed dosing in the humanized model where we tested our therapeutics on established tumors (80–100 mm^3,

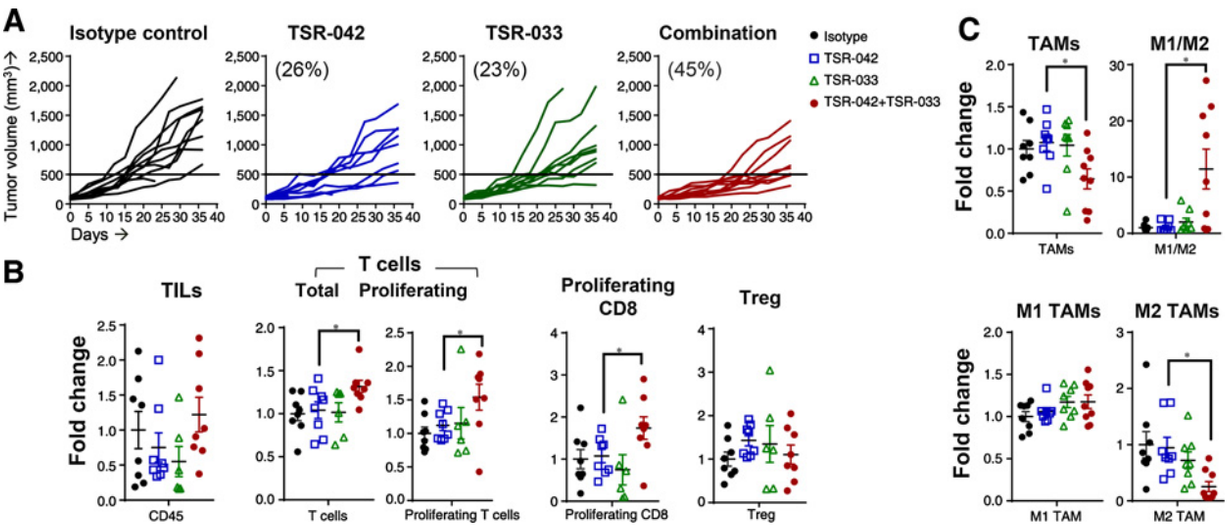

Figure 4.

Dual blockade of LAG-3 and PD-1 using TSR-033 and TSR-042 improves therapeutic efficacy and T-cell stimulation in a humanized NSCLC tumor mouse model. **A,** The combination of TSR-033 with TSR-042 has an additive effect (CDI = 1.001) on restricting tumor growth in HuNOG-EXL mice inoculated with A549 cells. Mice were randomized at tumor volumes of 80 to 120 mm^3, followed by administration of the indicated regimens (Materials and Methods). Tumor growth inhibition at termination for each treatment arm is indicated in parentheses. **B,** Relative to TSR-042 monotherapy, the combination group had increased intratumoral T cells and proliferating CD8 T cells; *, $P \leq 0.05$, unpaired Student *T* test. **C,** The combination of TSR-033 with TSR-042, compared with TSR-042 monotherapy, resulted in significant reduction in TAMs, M2 TAMs and increased M1/M2 ratios. TAMs were identified as $CD45^+CD3^-CD20^-CD68^+$, M2 TAMS, $CD45^+CD3^-CD20^-CD68^+HLA\text{-}DR^{lo}CD209^+$, and M1 TAMs, $CD45^+CD3^-CD20^-CD68^+HLA\text{-}DR^{hi}CD209^-$. Data represent two independent experiments ($n = 10$ per treatment arm) and have been normalized to fold change over isotype control for each treatment arm in **B**; *, $P \leq 0.05$, unpaired Student *T* test.

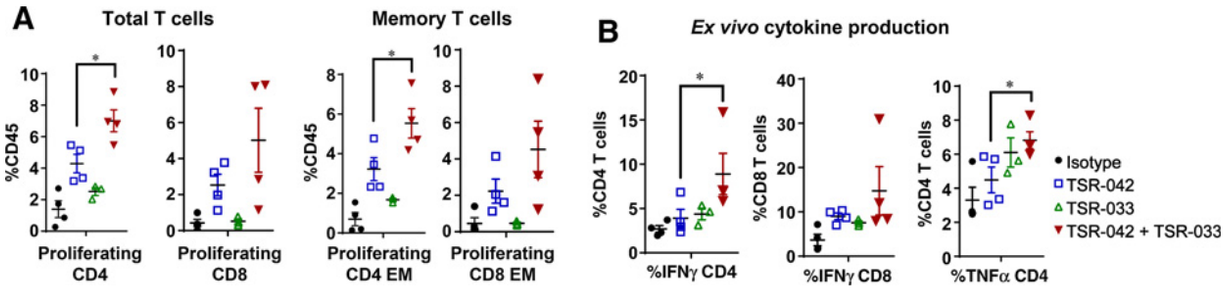

Figure 5.
Increased effector-memory T cells and *ex vivo* cytokine production by splenic T cells from the combination group, relative to TSR-042 alone in a humanized NSCLC tumor mouse model. **A,** Increase in proliferating and effector-memory ($CD45RA^{-}CCR7^{-}$) CD4 and CD8 T cells in the combination group compared with TSR-042 alone. **B,** Significant increase in IFNγ and TNFα production by CD4 T cells in the combination group over TSR-042 alone, upon *ex vivo* stimulation of mouse splenocytes (Materials and Methods); *, $P \leq 0.05$, unpaired Student *T* test.

compared with the A20 tumors at 30–50 mm^3 when dosing commenced; Materials and Methods).

Increased immuno-stimulation with combination therapy relative to PD-1 blockade alone

In line with the observed antitumor effect of the combination arm, there was a significant increase in total and proliferating intratumoral T cells, including CD8 T cells, in the combination arm relative to TSR-042 monotherapy (Fig. 4B). Overall TIL and regulatory T cell (Treg) frequencies were not significantly altered (Fig. 4B). Interestingly, combined blockade of PD-1 and LAG-3 also impinged on the myeloid compartment, reducing the overall frequency of tumor-associated macrophages (TAM), particularly the traditionally immunosuppressive M2 TAMs, skewing the balance between the more proinflammatory M1 TAMs relative to M2, resulting in higher M1/M2 ratios (Fig. 4C; refs. 45–47).

Combination treatment also led to increased splenic T-cell proliferation, with significant increases in proliferating CD4 and CD4 effector-memory T cells relative to TSR-042 monotherapy; proliferating CD8 and CD8 effector-memory T cells were also elevated in the combination group but this trend did not reach significance (Fig. 5A). Further, *ex vivo* stimulation of splenocytes with phorbol myristate acetate (PMA)/ionomycin, a common T-cell stimulus, yielded higher percentages of IFNγ- and TNFα-producing T cells in animals dosed with combination therapy (Fig. 5B), suggesting increased functional invigoration of T cells in the combination group relative to TSR-042.

Increased LAG-3 expression following PD-1 blockade

LAG-3 is coordinately expressed with PD-1 in numerous tumor types, and is reportedly upregulated on T cells postinhibition of the PD(L)-1 axis (48, 49). In our humanized mouse NSCLC model, LAG-3 was significantly upregulated on T cells in both tumors and spleens following TSR-042 monotherapy (Fig. 6A). LAG-3 positive T cells were especially impaired in their ability to produce IL2 upon *ex vivo* stimulation, compared with LAG-3 negative T cells, most strikingly within tumors, but also in spleens from both isotype control and TSR-042 treatment groups (Fig. 6B). IFNγ was not similarly affected (Fig. 6C). Loss of IL2 in parallel with retention of IFNγ production by $LAG\text{-}3^{+}$ dysfunctional CD8 TILs has been previously described, with IFNγ being

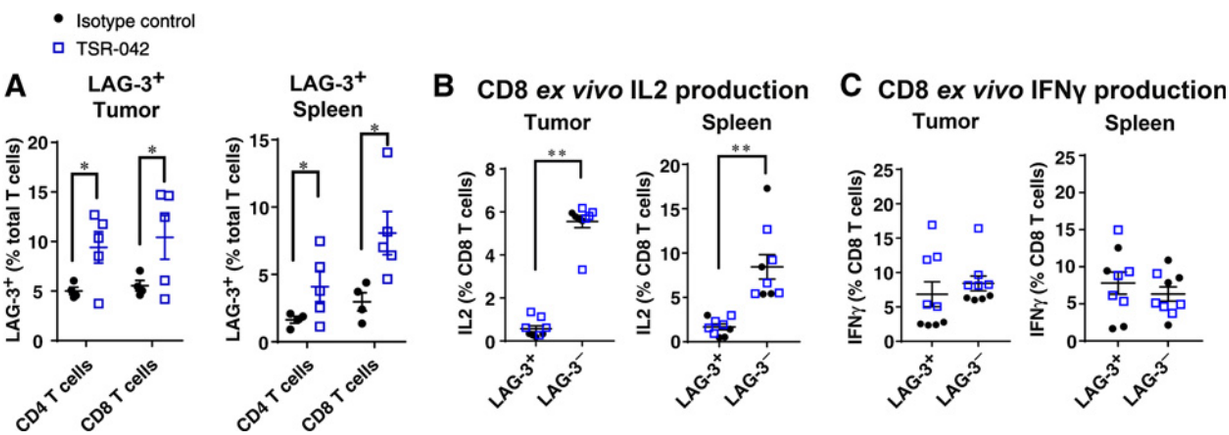

Figure 6.
Secondary upregulation of LAG-3 following PD-1 blockade. **A,** Significant increase in LAG-3 expression on T cells within A549 tumors and spleens of humanized NOG-EXL mice following TSR-042 treatment, relative to isotype control (end of study). Significant reduction in (**B**) IL2 production but not (**C**) IFNγ production by intratumoral and splenic LAG-3–positive T cells in both the isotype control and TSR-042 groups; *, $P \leq 0.05$; **, $P \leq 0.01$, unpaired Student *T* test.

ascribed an immunosuppressive role in this context through the downstream induction of molecules such as PD-L1 and IDO, contributing to adaptive resistance (50, 51).

Discussion

LAG-3 is associated with the attenuation of T-cell activation and function in the context of human cancers, establishing it as a promising immunotherapeutic target which is currently under clinical investigation (36). Preclinical studies in syngeneic mouse tumor models have demonstrated cooperativity between LAG-3 and PD-1 blockade in improving antitumor efficacy (4, 5, 36). We have extended these studies to B-cell malignancies, *vis-à-vis*, the mouse A20 lymphoma model to demonstrate that antibodies targeting LAG-3 and PD-1 not only synergize to elicit strong antitumor activity and concomitant T-cell activation, but also engender immunologic memory (Fig. 1). Although we noted the generation of immunologic memory in a subset of animals treated with anti-PD-1 alone, animals in the combination group displayed increased frequencies of proliferating memory T cells, and IFNγ/TNFα producing T cells in their spleens post-rechallenge, consistent with an amplified T-cell response (Fig. 1D).

TSR-033 is a humanized anti-LAG-3 antibody, generated from a mouse hybridoma selected on the basis of (i) high affinity binding to human and cyno LAG-3, (ii) the ability to block binding of a LAG-3 fusion protein to MHC Class II-expressing Daudi cells, and (ii) augment IL2 production by T cells in an MLR assay (Figs. 2 and 3; Table 1). We further confirmed the functional activity of TSR-033 using two separate *in vitro* T-cell stimulation assays, using either a NFAT-luciferase reporter cell line or a SEB-driven superantigen assay for T-cell activation (Figs. 2D and 3). TSR-033 showed no binding to C1q or the FcR family member CD16a in comparison with a human IgG1 positive control (Supplementary Fig. S4; Supplementary Table S2), confirming that it is unlikely to elicit either complement-dependent cytotoxicity or antibody-dependent cell cytotoxicity.

To test the *in vivo* antitumor efficacy of LAG-3 blockade with TSR-033, we used a humanized mouse model NOG-EXL, wherein human hematopoietic stem cells (HSC) are engrafted into severely immunodeficient NOG-EXL mice, which support the expansion of both lymphocytic and myeloid populations derived from the human HSCs (32). Monotherapy with either TSR-042 or TSR-033 had limited effect on the growth of established tumors derived from the A549 human NSCLC cell line (Fig. 4A). The combination of PD-1 and LAG-3 blockade improved antitumor efficacy, having an additive effect on growth inhibition of established A549 tumors (Fig. 4A). Our results represent the first demonstration, to the best of our knowledge, of the therapeutic benefit of anti-PD-1+anti-LAG-3 combination treatment in a humanized mouse model of NSCLC, helping provide insights into immune mechanisms promoting or subverting tumor clearance in a human cancer setting.

Consistent with increased antitumor efficacy, combined treatment with TSR-042 and TSR-033 led to significant increases in total and proliferating intratumoral T cells and proliferating CD8 T cells, compared with TSR-042 treatment alone, indicative of an enhanced T-cell response (Fig. 4B). Along similar lines, splenic CD4 T cells from animals given combination therapy yielded significantly higher frequencies of IFNγ and TNFα producers upon *ex vivo* stimulation (the trend did not reach significance for CD8 T cells; Fig. 5B). Further, the combination therapy arm also yielded a higher proportion of proliferating CD4 and CD8 effector-memory T cells (Fig. 5A). Interestingly, combined blockade also led to a reduction in TAMs, particularly the more immunosuppressive M2 TAMs (Fig. 4C). Whether this arises from direct inhibition of PD-1/LAG-3 expressed on TAMs, or occurs as a consequence of improved T-cell activation which would be expected to skew the balance in favor of the more pro-inflammatory M1 TAMs (47) remains to be determined.

Finally, the percentage of LAG-3^+ T cells was significantly increased following PD-1 monotherapy in the humanized NSCLC mouse model, likely curtailing the full extent of immuno-stimulation elicited by PD-1 blockade alone (Fig. 6A). Intratumoral LAG-3 positive T cells were particularly diminished in IL2 production compared with LAG-3 negative T cells, suggesting a reduction in functional and proliferative capacity (Fig. 6B; ref. 50). Adaptive upregulation of checkpoints such as LAG-3, in response to PD-1 blockade, along with numerous reports of coexpression with PD-1, reinforce the rationale for dual PD-1 and LAG-3 inhibitor combinations, which if tolerated, could result in more robust invigoration of the immune response and ultimately, more effective tumor eradication.

Disclosure of Potential Conflicts of Interest

J. Choi has ownership interest (including stock, patents, etc.) in AnaptysBio, Inc. H.T. Jun has ownership interest (including stock, patents, etc.) in AnaptysBio, Inc. M. Kehry is an Executive Director at AnaptysBio, Inc.; reports receiving commercial research grant from AnaptysBio, Inc.; and has ownership interest (including stock, patents, etc.) in AnaptysBio, Inc. S. Ramaswamy has ownership interest (including stock, patents, etc.) in TESARO. D. Jenkins works for and has ownership interest (including stock, patents, etc.) in TESARO.

Authors' Contributions

Conception and design: S. Ghosh, G. Sharma, S. Kumar, H.T. Jun, S. Ramaswamy, D. Jenkins
Development of methodology: G. Sharma, S. Kumar, H.T. Jun, D. Jenkins
Acquisition of data (provided animals, acquired and managed patients, provided facilities, etc.): G. Sharma, J. Travers, S. Kumar, J. Choi, H.T. Jun, M. Kehry
Analysis and interpretation of data (e.g., statistical analysis, biostatistics, computational analysis): S. Ghosh, G. Sharma, J. Travers, S. Kumar, J. Choi, D. Jenkins
Writing, review, and/or revision of the manuscript: S. Ghosh, G. Sharma, S. Kumar, H.T. Jun, M. Kehry, S. Ramaswamy, D. Jenkins
Administrative, technical, or material support (i.e., reporting or organizing data, constructing databases): J. Choi
Study supervision: S. Ghosh, G. Sharma, M. Kehry, S. Ramaswamy, D. Jenkins

Acknowledgments

Editorial support was provided by Anne Cooper and Dena McWain of Ashfield Healthcare Communications, Middletown, CT, and coordinated by Hemant Vyas, PhD, of TESARO, Inc.

The costs of publication of this article were defrayed in part by the payment of page charges. This article must therefore be hereby marked *advertisement* in accordance with 18 U.S.C. Section 1734 solely to indicate this fact.

Received July 30, 2018; revised September 25, 2018; accepted December 18, 2018; published first December 26, 2018.

References

1. Wherry EJ. T cell exhaustion. Nat Immunol 2011;12:492–9.
2. Philip M, Fairchild L, Sun L, Horste EL, Camara S, Shakiba M, et al. Chromatin states define tumour-specific T cell dysfunction and reprogramming. Nature 2017;545:452–6.
3. Huang AC, Postow MA, Orlowski RJ, Mick R, Bengsch B, Manne S, et al. T-cell invigoration to tumour burden ratio associated with anti-PD-1 response. Nature 2017;545:60–5.
4. Anderson AC, Joller N, Kuchroo VK. Lag-3, Tim-3, and TIGIT: co-inhibitory receptors with specialized functions in immune regulation. Immunity 2016;44:989–1004.
5. Nguyen LT, Ohashi PS. Clinical blockade of PD1 and LAG3–potential mechanisms of action. Nat Rev Immunol 2015;15:45–56.
6. Huard B, Gaulard P, Faure F, Hercend T, Triebel F. Cellular expression and tissue distribution of the human LAG-3-encoded protein, an MHC class II ligand. Immunogenetics 1994;39:213–7.
7. Triebel F, Jitsukawa S, Baixeras E, Roman-Roman S, Genevee C, Viegas-Pequignot E, et al. LAG-3, a novel lymphocyte activation gene closely related to CD4. J Exp Med 1990;171:1393–405.
8. Huard B, Prigent P, Tournier M, Bruniquel D, Triebel F. CD4/major histocompatibility complex class II interaction analyzed with CD4- and lymphocyte activation gene-3 (LAG-3)-Ig fusion proteins. Eur J Immunol 1995;25:2718–21.
9. Xu F, Liu J, Liu D, Liu B, Wang M, Hu Z, et al. LSECtin expressed on melanoma cells promotes tumor progression by inhibiting antitumor T-cell responses. Cancer Res 2014;74:3418–28.
10. Huard B, Mastrangeli R, Prigent P, Bruniquel D, Donini S, El-Tayar N, et al. Characterization of the major histocompatibility complex class II binding site on LAG-3 protein. Proc Natl Acad Sci U S A 1997;94:5744–9.
11. Matsuzaki J, Gnjatic S, Mhawech-Fauceglia P, Beck A, Miller A, Tsuji T, et al. Tumor-infiltrating NY-ESO-1-specific CD8+ T cells are negatively regulated by LAG-3 and PD-1 in human ovarian cancer. Proc Natl Acad Sci U S A 2010;107:7875–80.
12. Camisaschi C, Casati C, Rini F, Perego M, De Filippo A, Triebel F, et al. LAG-3 expression defines a subset of CD4(+)CD25(high)Foxp3(+) regulatory T cells that are expanded at tumor sites. J Immunol 2010;184:6545–51.
13. Joller N, Kuchroo VK. Tim-3, Lag-3, and TIGIT. Curr Top Microbiol Immunol 2017;410:127–56.
14. Thommen DS, Schreiner J, Muller P, Herzig P, Roller A, Belousov A, et al. Progression of lung cancer is associated with increased dysfunction of T cells defined by coexpression of multiple inhibitory receptors. Cancer Immunol Res 2015;3:1344–55.
15. Baitsch L, Baumgaertner P, Devevre E, Raghav SK, Legat A, Barba L, et al. Exhaustion of tumor-specific CD8(+) T cells in metastases from melanoma patients. J Clin Invest 2011;121:2350–60.
16. Norstrom MM, Radestad E, Sundberg B, Mattsson J, Henningsohn L, Levitsky V, et al. Progression of benign prostatic hyperplasia is associated with pro-inflammatory mediators and chronic activation of prostate-infiltrating lymphocytes. Oncotarget 2016;7:23581–93.
17. Angevin E, Kremer F, Gaudin C, Hercend T, Triebel F. Analysis of T-cell immune response in renal cell carcinoma: polarization to type 1-like differentiation pattern, clonal T-cell expansion and tumor-specific cytotoxicity. Int J Cancer 1997;72:431–40.
18. Huang RY, Eppolito C, Lele S, Shrikant P, Matsuzaki J, Odunsi K. LAG3 and PD1 co-inhibitory molecules collaborate to limit CD8+ T cell signaling and dampen antitumor immunity in a murine ovarian cancer model. Oncotarget 2015;6:27359–77.
19. Woo SR, Turnis ME, Goldberg MV, Bankoti J, Selby M, Nirschl CJ, et al. Immune inhibitory molecules LAG-3 and PD-1 synergistically regulate T-cell function to promote tumoral immune escape. Cancer Res 2012;72:917–27.
20. Weber JS, Hodi FS, Wolchok JD, Topalian SL, Schadendorf D, Larkin J, et al. Safety profile of nivolumab monotherapy: a pooled analysis of patients with advanced melanoma. J Clin Oncol 2017;35:785–92.
21. Topalian SL, Hodi FS, Brahmer JR, Gettinger SN, Smith DC, McDermott DF, et al. Safety, activity, and immune correlates of anti-PD-1 antibody in cancer. N Engl J Med 2012;366:2443–54.
22. Topalian SL, Drake CG, Pardoll DM. Immune checkpoint blockade: a common denominator approach to cancer therapy. Cancer Cell 2015;27:450–61.
23. Sharma P, Hu-Lieskovan S, Wargo JA, Ribas A. Primary, adaptive, and acquired resistance to cancer immunotherapy. Cell 2017;168:707–23.
24. Baudino L, Shinohara Y, Nimmerjahn F, Furukawa J, Nakata M, Martinez-Soria E, et al. Crucial role of aspartic acid at position 265 in the CH2 domain for murine IgG2a and IgG2b Fc-associated effector functions. J Immunol 2008;181:6664–9.
25. Yamazaki T, Akiba H, Koyanagi A, Azuma M, Yagita H, Okumura K. Blockade of B7-H1 on macrophages suppresses CD4+ T cell proliferation by augmenting IFN-gamma-induced nitric oxide production. J Immunol 2005;175:1586–92.
26. Workman CJ, Rice DS, Dugger KJ, Kurschner C, Vignali DA. Phenotypic analysis of the murine CD4-related glycoprotein, CD223 (LAG-3). Eur J Immunol 2002;32:2255–63.
27. Bowers PM, Horlick RA, Neben TY, Toobian RM, Tomlinson GL, Dalton JL, et al. Coupling mammalian cell surface display with somatic hypermutation for the discovery and maturation of human antibodies. Proc Natl Acad Sci U S A 2011;108:20455–60.
28. Horlick RA, Macomber JL, Bowers PM, Neben TY, Tomlinson GL, Krapf IP, et al. Simultaneous surface display and secretion of proteins from mammalian cells facilitate efficient in vitro selection and maturation of antibodies. J Biol Chem 2013;288:19861–9.
29. Laken H, Kehry M, McNeeley P, Neben T, Zhang J, Jenkins D, et al. Identification and characterization of TSR-042, a novel anti-human PD-1 therapeutic antibody. Eur J Cancer 2016;69:S102.
30. Ito M, Hiramatsu H, Kobayashi K, Suzue K, Kawahata M, Hioki K, et al. NOD/SCID/gamma(c)(null) mouse: an excellent recipient mouse model for engraftment of human cells. Blood 2002;100:3175–82.
31. Verma B, Mancini M, Davies A, Sidransky D, Goodwin N. Abstract A016: NOG-EXL mice have superior immune cell engraftment and lineage development in the human immune system (HIS) model, the ImmunoGraft. Mol Cancer Ther 2018;17(1 Suppl):A016.
32. Ito R, Takahashi T, Katano I, Kawai K, Kamisako T, Ogura T, et al. Establishment of a human allergy model using human IL-3/GM-CSF-transgenic NOG mice. J Immunol 2013;191:2890–9.
33. Foster KA, Oster CG, Mayer MM, Avery ML, Audus KL. Characterization of the A549 cell line as a type II pulmonary epithelial cell model for drug metabolism. Exp Cell Res 1998;243:359–66.
34. Xu W, Bi Y, Zhang J, Kong J, Jiang H, Tian M, et al. Synergistic antitumor efficacy against the EGFRvIII+HER2+ breast cancers by combining trastuzumab with anti-EGFRvIII antibody CH12. Oncotarget 2015;6:38840–53.
35. Kim H, George E, Ragland R, Rafial S, Zhang R, Krepler C, et al. Targeting the ATR/CHK1 axis with PARP inhibition results in tumor regression in BRCA-mutant ovarian cancer models. Clin Cancer Res 2017;23:3097–108.
36. Andrews LP, Marciscano AE, Drake CG, Vignali DA. LAG3 (CD223) as a cancer immunotherapy target. Immunol Rev 2017;276:80–96.
37. Tang H, Liang Y, Anders RA, Taube JM, Qiu X, Mulgaonkar A, et al. PD-L1 on host cells is essential for PD-L1 blockade-mediated tumor regression. J Clin Invest 2018;128:580–8.
38. Silva JP, Vetterlein O, Jose J, Peters S, Kirby H. The S228P mutation prevents in vivo and in vitro IgG4 Fab-arm exchange as demonstrated using a combination of novel quantitative immunoassays and physiological matrix preparation. J Biol Chem 2015;290:5462–9.
39. Baixeras E, Huard B, Miossec C, Jitsukawa S, Martin M, Hercend T, et al. Characterization of the lymphocyte activation gene 3-encoded protein. A new ligand for human leukocyte antigen class II antigens. J Exp Med 1992;176:327–37.
40. Shapiro M, Herishanu Y, Katz BZ, Dezorella N, Sun C, Kay S, et al. Lymphocyte activation gene 3: a novel therapeutic target in chronic lymphocytic leukemia. Haematologica 2017;102:874–82.
41. Banchereau J, Palucka AK. Dendritic cells as therapeutic vaccines against cancer. Nat Rev Immunol 2005;5:296–306.
42. Sabins NC, Harman BC, Barone LR, Shen S, Santulli-Marotto S. Differential expression of immune checkpoint modulators on in vitro primed CD4(+) and CD8(+) T cells. Front Immunol 2016;7:221.
43. Sachdev JC, Patnaik A, Waypa J, Pelusi J, Beeram M, Im E, et al. 1185PSafety, pharmacodynamic, and pharmacokinetic profile of TSR-042, an anti–PD–1

monoclonal antibody, in patients (pts) with advanced solid tumors. Ann Oncol 2017;28 (Suppl 5):mdx376.050.
44. He Y, Yu H, Rozeboom L, Rivard CJ, Ellison K, Dziadziuszko R, et al. LAG-3 protein expression in non-small cell lung cancer and its relationship with PD-1/PD-L1 and tumor-infiltrating lymphocytes. J Thorac Oncol 2017;12: 814–23.
45. Almatroodi SA, McDonald CF, Darby IA, Pouniotis DS. Characterization of M1/M2 tumour-associated macrophages (TAMs) and Th1/Th2 cytokine profiles in patients with NSCLC. Cancer Microenviron 2016;9:1–11.
46. Yuan A, Hsiao YJ, Chen HY, Chen HW, Ho CC, Chen YY, et al. Opposite effects of M1 and M2 macrophage subtypes on lung cancer progression. Sci Rep 2015;5:14273.
47. de Groot AE, Pienta KJ. Epigenetic control of macrophage polarization: implications for targeting tumor-associated macrophages. Oncotarget 2018;9:20908–27.
48. Koyama S, Akbay EA, Li YY, Herter-Sprie GS, Buczkowski KA, Richards WG, et al. Adaptive resistance to therapeutic PD-1 blockade is associated with upregulation of alternative immune checkpoints. Nat Commun 2016;7: 10501.
49. Huang RY, Francois A, McGray AR, Miliotto A, Odunsi K. Compensatory upregulation of PD-1, LAG-3, and CTLA-4 limits the efficacy of single-agent checkpoint blockade in metastatic ovarian cancer. Oncoimmunology 2017;6:e1249561.
50. Williams JB, Horton BL, Zheng Y, Duan Y, Powell JD, Gajewski TF. The EGR2 targets LAG-3 and 4-1BB describe and regulate dysfunctional antigen-specific CD8+ T cells in the tumor microenvironment. J Exp Med 2017; 214:381–400.
51. Spranger S, Spaapen RM, Zha Y, Williams J, Meng Y, Ha TT, et al. Up-regulation of PD-L1, IDO, and T(regs) in the melanoma tumor microenvironment is driven by CD8(+) T cells. Sci Transl Med 2013;5:200ra116.